

# FIBER RECOGNITION IN COMPOSITE MATERIALS

Xiang Li, Sara Shonkwiler, Sara McMains

University of California, Berkeley

## ABSTRACT

The accuracy of fiber recognition in cross-sectional scanned images is critical to material characterization for Fiber-Reinforced Polymer (FRP) composites. It is challenging to accurately detect and locate all fibers, especially broken fibers. We propose a two-step approach to automatically detect and categorize fibers. First we exploit distance-transform-based watershed segmentation to extract the boundaries of individual fiber cross-sections to handle cases where fibers contact each other, then use our proposed contour gradient charts to evaluate the breakage of each fiber cross-section and classify individual fiber boundaries as circles or ellipses. Our method accurately and robustly recognizes fibers in the cross-sectional images, whether they are aligned or misaligned, complete or broken.

**Index Terms**— Fiber recognition, Microscope image processing, Circle detection, Shape analysis, Fiber-reinforced polymer

## 1. INTRODUCTION

Fiber-reinforced polymer (FRP) composites are one of the most popular composite materials, widely used in aerospace, automotive, and other manufacturing industries [1] because of their superior strength-to-weight ratio. The constituents of FRP materials are the fibers, which provide the majority of the strength and stiffness of the material; and the polymer matrix, which binds the fibers together. The properties of FRP materials are largely dependent on their microstructure, such as the geometric distribution of the fibers in the matrix. To characterize FRP materials and inspect their microstructure, one of the most common approaches is to analyze cross-sectional scanned images either by optical microscopy [2] or computed tomography [3] of the composite materials.

In this paper, we will consider the case of unidirectional FRP composites (see a sparse example in Fig. 1 and an actual cross-section in Fig. 2). In these composites, most fibers are aligned, which provides the FRP part extraordinary mechanical performance along this major fiber direction. For material characterization, researchers analyze cross-sectional scans taken transversely to the major fiber direction, in which aligned fibers will appear as circles, and misaligned fibers appear as ellipses (Fig. 1(b)).

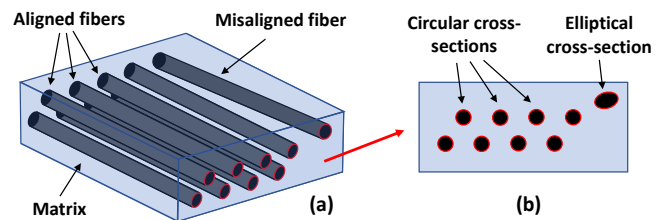


**Fig. 1.** Diagram of (a) a unidirectional FRP composite; (b) its transverse cross-section with aligned and misaligned fiber cross-sections appearing as circles and ellipses respectively.

The scanned images enable researchers to analyze the basic composite properties, assess microstructural damage [2], and reconstruct three-dimensional microstructure [4, 5]. All of these material characterization analyses rely on the accuracy of fiber recognition from the scanned images. The characterization can not be accurate if the fibers are not correctly identified and located in the images.

Recognizing fibers from the scanned image usually follows a two-step process: (1) segment fibers that contact each other into individual fiber pixel blob regions; (2) fit a circle or an ellipse to each individual fiber pixel blob. Mlekusch [6] separated the touching fiber regions into individual fiber segments based on their convexity, and then fitted contour points of each segment into ellipses based on a regression calculation. In [7], Martin-Herrero et al. detected individual fiber blobs by using successive mathematical morphology operations, and then fitted ellipses to them based on least-squares orthogonal distance fitting [8]. Amjad et al. [5] applied a marker-controlled watershed segmentation to identify fibers, and then approximated them as ellipses by a Hough-transform-based ellipse detector [9]. The above methods performed well under the assumption that all the fibers are undamaged fibers (circles or ellipses); however, broken fibers are common in FRP composites (Fig. 2). An accurate method to recognize both the broken and complete fibers is necessary and is crucial to the overall evaluation of the composite material.

We present a novel method to automatically recognize fibers in composite material cross-sectional images, whether they are aligned or misaligned, complete or broken. This method first segments the binarized scanned image into individual fiber pixel blobs using watershed segmentation, and

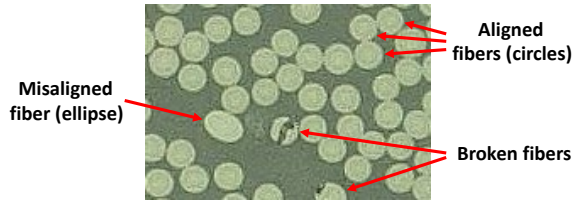


**Fig. 2.** An example of the input scanned image

then identifies their breakage and fits circles or ellipses to them. To better identify the fiber breakage, we introduce a new method, called contour gradient charts, that efficiently distinguishes complete and broken fibers and further helps with the circle/ellipse fitting.

## 2. FIBER BLOB DETECTION

Since the fiber cross-sections all appear as complete or broken circular/elliptical blobs in the scanned image, we first detect blob areas for each individual fiber. Fig. 3 illustrates the steps of our fiber blob detection process: (a) converting the input image to grayscale; (b) binarizing the grayscale image and removing noise; (c) building the distance transform from the binary image; (d) applying watershed segmentation on the distance transform; (e) merging oversegmented regions; (f) result: individual fiber pixel blobs.

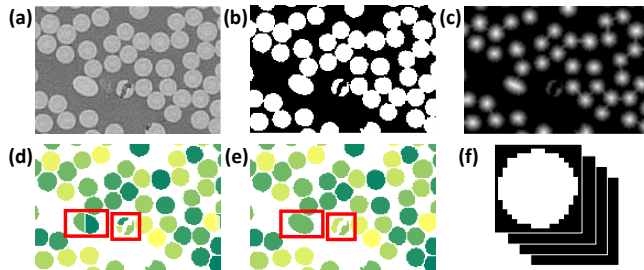


**Fig. 3.** The procedure for fiber blob detection: (a) grayscale; (b) binarization and cleaning; (c) distance transform; (d) watershed segmentation; (e) merging oversegmented regions; (f) result: individual fiber pixel blobs.

Beginning with the original scanned image, we convert it to grayscale and apply Gaussian smoothing to reduce noise (Fig. 3(a)). In the smoothed grayscale image, fiber pixels have observably higher intensity values than the resin matrix pixels. Based on the intensity contrast between fiber and matrix pixels, we convert the grayscale image into a binary image using Otsu's histogram-based global thresholding method [10] and denoise it (Fig. 3(b)). We do so by identifying connected fiber (white in the image) pixel regions below a minimum number of pixels. In our experiments, we found removing regions with fewer than 10 connected pixels (about 10% of fiber cross-section size) led to good fiber detection results.

After denoising, each individual connected fiber pixel region in the binary image corresponds to one of the following: an individual fiber, a group of contacting fibers, or a chunk of broken fiber. To segment individual fiber blobs from regions of contacting fibers, we exploit distance-transform-based watershed segmentation, as follows.

From the binary image, we build a Euclidean distance transform [11] that assigns each pixel its distance to the nearest polymer (matrix) pixel (Fig. 3(c)). The local maximum values in the distance transform efficiently indicate the centers of each individual fiber. We then run watershed segmentation [12] on the distance transform, separating contacting fibers into individual fiber blobs (Fig. 3(d)).

In the continuous space, perfect circles and ellipses only have one local maximum distance point at their centers. However, since the composite images are represented in discrete pixels, the fibers are not perfect circles or ellipses, which may cause multiple local maxima being calculated near the fiber center point. As illustrated in Fig. 3(d) left red box, this can cause an oversegmentation in the watershed segmentation. Broken fibers may also be oversegmented because of their irregular shapes (Fig. 3(d) right red box). To deal with these oversegmentation problems, after the watershed segmentation, we merge detected regions whose local maxima in the distance transform were close and that were also connected in the binary image (Fig. 3(e)).

The output of the fiber blob detection is pixel blobs representing detected individual fibers (Fig. 4). Next (Section 3), we will describe how we identify their breakage, and compute their locations accordingly.

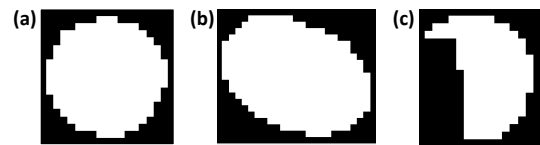


**Fig. 4.** Real-world examples of different fiber blob types: (a) complete aligned fiber; (b) complete misaligned fiber; (c) broken fiber.

## 3. FIBER BREAKAGE EVALUATION AND LOCALIZATION

After identifying the pixel blobs for each fiber, we propose a novel tool called contour gradient charts to help determine if they are broken. Based on the analysis from the contour gradient charts, we select unbroken contour pixels and fit a circle or ellipse to each fiber.

### 3.1. Breakage evaluation via contour gradient charts

Our approach to determining whether a fiber blob is broken or not is based on a simple yet powerful idea: for complete

fiber blobs, the gradient direction along the boundary varies smoothly along all its contour pixels; for broken fiber blobs, the gradient direction varies smoothly only along the contour pixels bounding its unbroken portion, but rapidly changes at the broken portion of the contour pixels. This property enables us to determine if a fiber blob is broken by checking if rapid gradient changes exist along its contour pixels.

We define the gradient direction of a boundary point (assuming a continuous perfect circle for illustration) to be perpendicular to its tangent line and into the circle. An example is illustrated in Fig. 5, where twelve points are evenly sampled on the circle in clockwise order (from  $P_1$  to  $P_{12}$ ), with gradient directions for examples  $P_1$ ,  $P_5$ , and  $P_{10}$  shown.

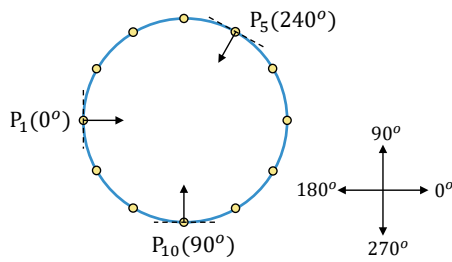


**Fig. 5.** An example of contour sample points and their gradient directions.

We create a “Contour Gradient Chart” (CGC) to illustrate the gradient direction change along the boundary sample points. In the chart, x values are the sample points on the contour of the circle in clockwise order and y values are their corresponding gradient direction angles (Fig. 6(a)). To analyze the rate of change of gradient angles, we take the derivative (numerical gradient) of the CGC modulo  $360^\circ$  and call it the “first derivative CGC” (Fig. 6(b)).

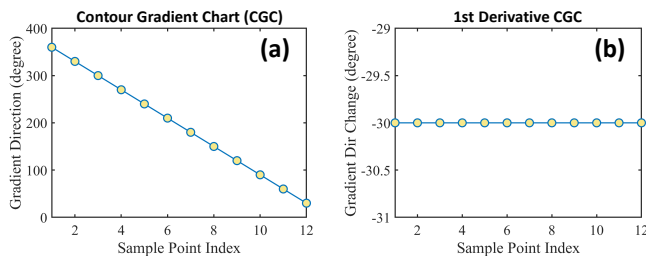


**Fig. 6.** Contour gradient charts of the example in Fig. 5.

Now considering the fiber blobs detected from Section 2, we construct CGCs of each by selecting their contour (boundary) pixels as the sample points. For these contour pixels, we use the Sobel-Feldman operator to calculate their gradient vectors. The discretized contour pixels bring noise to the calculation of the gradient, but after applying a moving average operation, the gradient direction changes between sample points on complete fibers are small and approximately constant because of the smoothness of complete circles and el-

lipses (Fig. 7). Call the number of sample points  $N$ . The sum of all the signed gradient direction changes will total  $360^\circ$  along all boundary pixels, so the average value of gradient direction changes, which should be close to the approximately constant value for unbroken fibers, is  $-360^\circ/N$  in the first derivative CGC.

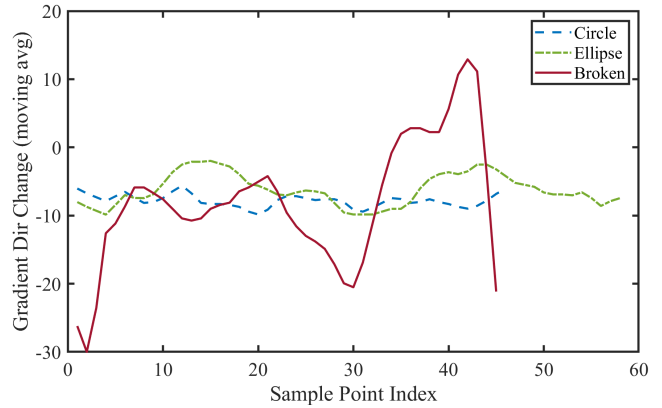


**Fig. 7.** Example first derivative CGC of fiber blobs from Fig. 4. The circular, elliptical, and broken fibers have  $N_C=46$ ,  $N_E=58$ , and  $N_B=45$  boundary pixels, respectively. Complete fibers (circle/ellipse) have relatively steady gradient direction changes close to  $-360^\circ/N_C = -7.8^\circ$  or  $-360^\circ/N_E = -6.2^\circ$ ; the broken fiber has dramatic changes far from  $-360^\circ/N_B = -8^\circ$ .

However, for broken fibers, dramatic gradient direction changes occur at the break points. It is easy to observe and classify the broken fibers and complete fibers from their first derivative CGCs by detecting if there are large gradient direction changes or not (Fig. 7 and 8). Furthermore, the unbroken portion of the contour can be identified using the first derivative CGC. Similar to a complete fiber blob, the corresponding range of the unbroken portion of a broken fiber would be seen as a long period of approximately constant gradient changes around  $-360^\circ/N$  in the first derivative CGC (Fig. 8).

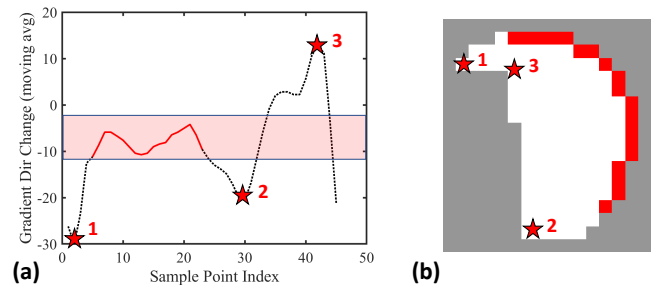


**Fig. 8.** Selected unbroken portion of contours are shown in red in (a) first derivative CGC, and (b) its corresponding fiber blob. Red stars demonstrate dramatic gradient direction changes and their relations to the actual break points.

### 3.2. Circle and ellipse fitting

The final step is to fit a circle or an ellipse to the candidate contour pixels of each fiber blob. For complete fibers, all of their blob boundary pixels are taken as the candidate pixels; for broken fibers, only the selected unbroken portion of boundary pixels are the candidate pixels.

Since a circle is a special case of an ellipse, we choose to apply a direct ellipse fitting algorithm [13] to our candidate pixels in order to simultaneously handle both aligned and misaligned fibers (Fig. 9).

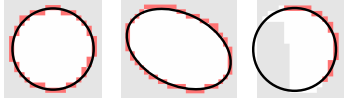


**Fig. 9.** Circle/ellipse fitting results for different fiber blob types. The input pixels are rendered in light red.

## 4. EXPERIMENTAL RESULTS

We tested our proposed method on more than 30 real-world microscope cross-sectional images from 3D printed FRP parts. The images have an average size of 18,000\*9,500 pixels and contain about 500,000 carbon fiber cross-sections, with 7-8% broken fibers. The categorization and localization (the calculation of fiber boundaries) output of our algorithm on the test images was manually examined by material experts, who found no errors with our method's results for almost all fibers (>99.9% overall correctness, >99% correctness for broken fibers). Typical classification failures occur when the breakage is fully inside a fiber, or an inclusion with nearly smooth contour exists (Fig. 11(a, c)). In such cases, since no rapid gradient changes exist along the fiber boundaries, our algorithm falsely identifies them as complete fibers (Fig. 11(b, d)).

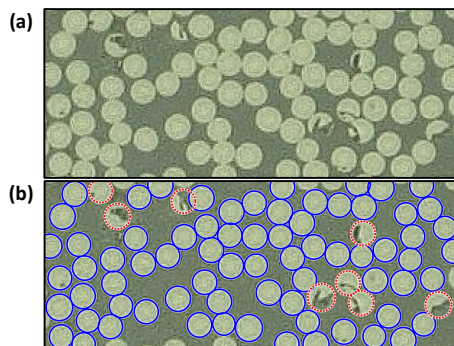


**Fig. 10.** Experimental results: (a) the input image; (b) recognized complete (blue) and broken (red dotted) fibers.

To the best of our knowledge, our approach is the first method that can robustly recognize broken fibers and cal-

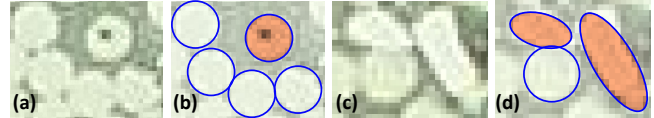


**Fig. 11.** Failure cases: (a-b) a broken fiber with only inner breakage is falsely identified as a complete fiber; (c-d) (two) inclusions falsely identified as complete misaligned fibers. (Incorrect identifications are shaded beige.)

culate their fitting circles/ellipses. In contrast, direct circle/ellipse detection methods [9, 14] are generally based on the theory of the Hough transform, which is sensitive to noise. Because there is often fiber debris (noisy pixels) around the breakage locations, the direct detection methods are prone to generate false positive detections around the broken fibers (Fig.12(b)). Fiber blob segmentation and ellipse fitting methods [5, 6, 7] efficiently eliminate the noisy pixels by the blob segmentation process, but they are unable to recognize breakage in the fibers. The contour pixels on the broken portion may cause inaccurate circle/ellipse fitting (Fig.12(c)). Our proposed method only selects contour pixels on the unbroken portion after eliminating noisy pixels during the fiber blob detection process, and only then fits ellipses to identify misaligned fibers. These operations lead to a more robust and accurate detection of the broken fibers (Fig.12(d)).

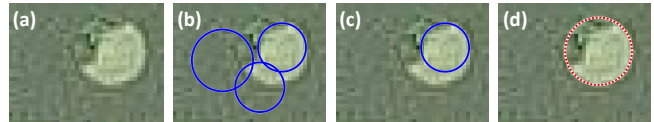


**Fig. 12.** Localization results comparison with other popular methods: (a) input; (b) direct circle/ellipse detection [9, 14]; (c) fiber blob segmentation and ellipse fitting [5, 6, 7]; (d) our method.

## 5. CONCLUSIONS

In this paper, we propose a novel fiber recognition algorithm, for cross-sectional scanned images of composite materials that detects all types of fibers and distinguish which are broken, unbroken, and/or misaligned. We introduce contour gradient charts, which enable identifying broken fibers as well which boundary pixels are on their unbroken contours, for more accurate circle and ellipse fitting. The performance is validated on real-world microscope images from 3D-printed fiber-reinforced polymer parts, on which our method is able to correctly identify and classify over 99.9% of fibers.

**Acknowledgements:** We gratefully acknowledge Arevo Inc. and Danning Zhang for valuable discussions and for providing the cross-sectional microscope images for testing; we thank Wei Wei for assistance with data preparation.

## 6. REFERENCES

- [1] Nekoda van de Werken, Halil Tekinalp, Pouria Khanbolouki, Soydan Ozcan, Andrew Williams, and Mehran Tehrani, "Additively manufactured carbon fiber-reinforced composites: State of the art and perspective," *Additive Manufacturing*, vol. 31, pp. 100962, 2020.
- [2] Brian S Hayes and Luther M Gammon, *Optical microscopy of fiber-reinforced composites*, ASM international, 2010.
- [3] Shenli Pei, Kaifeng Wang, Jingjing Li, Yang Li, Danielle Zeng, Xuming Su, Xianghui Xiao, and Hui Yang, "Mechanical properties prediction of injection molded short/long carbon fiber reinforced polymer composites using micro X-ray computed tomography," *Composites Part A: Applied Science and Manufacturing*, vol. 130, pp. 105732, 2020.
- [4] Youjie Zhou, Hongkai Yu, Jeff Simmons, Craig P Przybyla, and Song Wang, "Large-scale fiber tracking through sparsely sampled image sequences of composite materials," *IEEE Transactions on Image Processing*, vol. 25, no. 10, pp. 4931–4942, 2016.
- [5] K Amjad, WJR Christian, K Dvurecenska, MG Chapman, MD Uchic, CP Przybyla, and EA Patterson, "Computationally efficient method of tracking fibres in composite materials using digital image correlation," *Composites Part A: Applied Science and Manufacturing*, vol. 129, pp. 105683, 2020.
- [6] B Mlekusch, "Fibre orientation in short-fibre-reinforced thermoplastics II. Quantitative measurements by image analysis," *Composites Science and Technology*, vol. 59, no. 4, pp. 547–560, 1999.
- [7] Julio Martin-Herrero and Ch Germain, "Microstructure reconstruction of fibrous C/C composites from X-ray microtomography," *Carbon*, vol. 45, no. 6, pp. 1242–1253, 2007.
- [8] Sung Joon Ahn, Wolfgang Rauh, and Hans-Jürgen Warnecke, "Least-squares orthogonal distances fitting of circle, sphere, ellipse, hyperbola, and parabola," *Pattern Recognition*, vol. 34, no. 12, pp. 2283–2303, 2001.
- [9] Yonghong Xie and Qiang Ji, "A new efficient ellipse detection method," in *Object recognition supported by user interaction for service robots*. IEEE, 2002, vol. 2, pp. 957–960.
- [10] Nobuyuki Otsu, "A threshold selection method from gray-level histograms," *IEEE transactions on Systems, Man, and Cybernetics*, vol. 9, no. 1, pp. 62–66, 1979.
- [11] Calvin R Maurer, Rensheng Qi, and Vijay Raghavan, "A linear time algorithm for computing exact euclidean distance transforms of binary images in arbitrary dimensions," *IEEE Transactions on Pattern Analysis and Machine Intelligence*, vol. 25, no. 2, pp. 265–270, 2003.
- [12] Fernand Meyer, "Topographic distance and watershed lines," *Signal Processing*, vol. 38, no. 1, pp. 113–125, 1994.
- [13] Andrew Fitzgibbon, Maurizio Pilu, and Robert B Fisher, "Direct least square fitting of ellipses," *IEEE Transactions on Pattern Analysis and Machine Intelligence*, vol. 21, no. 5, pp. 476–480, 1999.
- [14] Tim J Atherton and Darren J Kerbyson, "Size invariant circle detection," *Image and Vision Computing*, vol. 17, no. 11, pp. 795–803, 1999.